PWR DOWNCOMER FLUID TEMPERATURE TRANSIENTS DUE TO HIGH PRESSURE INJECTION AT STAGNATED LOOP FLOW

by

T. G. Theofanous and H. P. Nourbakhsh

School of Nuclear Engineering
Purdue University
West Lafayette, Indiana 47907

September 1982

Presented at the Joint NRC/ANS Meeting on Basic Thermal Hydraulics Mechanisms in LWR Analysis September 14-15, 1982 at Bethesda, MD. 20014.

ABSTRACT

A simple, phenomena-oriented approach for the prediction of overcooling due to High Pressure Injection at zero loop flow is proposed. With the help of graphical representations for the decay of buoyant jets the prediction of the complete space-time temperature variations is reduced to simple hand calculations. Scaling aspects important in achieving adequate laboratory simulations of the reactor system are discussed.

1 INTRODUCTION

The purpose of this paper is to bring out the role of certain key physical processes that control the downcomer fluid temperature response to High Pressure Injection (HPI). The quantitative aspects of each one of these processes are first presented and a method for their integration into an overall predictive model is proposed. These predictions are compared to available experimental data including some of the more pertinent CREARE tests. Finally, predictions for a 3-loop Westinghouse PWR plant are presented. For simplicity we only consider the zero loop flow case here. Extension of the method to cases of non-stagnant loops will be considered in a separate paper.

2 THE PHYSICAL MODEL

2.1 Definitions and General Approach

We begin by *assuming* the existence of a stratified rather than well mixed flow regime. By "stratification" we mean non-uniformity in temperature, and density, in a direction transverse to the flow path, as qualitatively illustrated in Figure 1. The "hot" regions will be referred to as the "ambient" while the cold regions will be called "buoyant jets" or "stratified layers" if they are of vertical or horizontal orientation respectively. Stratification in a flowing system implies mixing and the mixing behavior of "buoyant jets" and of "stratified layers" is quite different. We identify therefore, mixing regions, MR's as shown in Figure 1 as the largest constitutive elements of the whole flow domain. The HPI flow first produces a buoyant jet (MR1), which is deflected into a horizontally flowing stratified layer (MR2) that spills over into the downcomer (MR3) forming another buoyant jet (MR4) as it descends into the lower plenum. The possibility of backflow into the pump and the loop seal must be mentioned here. However the magnitude of such flow will depend upon the details of the internal pump design and since the fluid mass associated with loop seal volume is normally small compared to the remaining volumes already considered (< 20%) such backflow beyond the pump will be conservatively neglected here.

If these mixing regions (stratification) indeed exist they would be established soon after the initiation of the HPI flow. Steady conditions,

would also be quickly approached and maintained indefinitely if the lower plenum was of infinite extent. The finite size of the lower plenum would cause a time-wise and space-wise variation of the "ambient." The mixing region response will, therefore, also vary correspondingly. We will show that space-wise variations of the ambient can be neglected and that time-wise variations are sufficiently slow to allow a simple quasi-static approach in treating individual mixing region responses. The question of existence of the mixing regions as portrayed in Figure 1 is considered, therefore, in the context of a uniform, steady, ambient.

2.2 The Existence of Mixing Regions

The question of existence of the stratified regime in the cold-leg (MR2) is one of *fundamental significance*. Its importance may be appreciated by considering the consequences of a perfectly mixed behavior instead Note that at zero loop flow all "forced" agitation takes place around the point of injection, i.e., *at most* the whole cold leg can be well mixed. In such a case we could predict the cold leg temperature transient by writing an energy balance over the cold leg with HPI flow entering at T_{HPI} and an equivalent volume outflow (into the downcomer) at the mixed mean temperature T_{CL}. We integrate by neglecting variations in cold leg mass due to density variation from ρ_{CLO} to ρ_{HPI}, we obtain:

$$\frac{T_{CL}-T_{HPI}}{T_{CL,0}-T_{HPI}} = e^{-\frac{Q_{HPI}}{V_{CL}}t} \qquad (1)$$

For a 3-loop W plant $V_{CL} \sim 160\,ft^3$, $Q_{HPI} \sim 0.5\,ft^3/s$, so that rapid cooldown with a time constant of 5 minutes to near HPI fluid temperatures ($\sim 60°F$) would be predicted. This cold fluid would enter the downcomer as a buoyant jet and it would have little chance to decay within the travel of the first few diameters. That is, very rapid cooldown would result in the first critical welds below the inlet nozzle.

A stratified regime, on the other hand, would allow a *local* decay of the HPI jet in MR1 with ambient fluid continuously drawn in from the downcomer (and lower plenum) along the cold leg and in counter-current flow

with the cold stratified layer beneath. This behavior is fundamentally different from that reflected in Equation (1) since a much larger volume of warm fluid (namely the whole lower plenum and downcomer, i.e., about 760 ft^3 corresponding to each loop) now has access to MR1. The time constant for changing the temperature of this "ambient" fluid is 25 minutes instead. Taking into account the heat stored in structures (i.e., vessel wall, lower plenum internals, etc.) the time constant would be even greater.

Our choice between these two fundamentally different regimes will be made on the basis of stability considerations. Specifically we will show that the perfectly mixed cold-leg regime is unstable and therefore it cannot exist, while no stability criteria are violated by the stratified regime.

Let us first consider the well mixed regime at, say, 5 minutes following HPI actuation. The cold leg will be filled by water at 240°F (ρ_{240} = 59.1 lb_m/ft^3) which is feeding the downcomer at the rate of 0.5 ft^3/s (0.117 ft/s). The downcomer ambient is at 550°F (ρ_{550} = 45.8 lb_m/ft^3) at this time. Under these conditions the characteristic length scale would be the cold-leg diameter (2.3 ft) yielding a local (at the cold leg/downcomer junction) Froude number of

$$Fr_o = \frac{U_{cl}}{\left(g D_{cl} \frac{\rho_{240} - \rho_{550}}{\rho_{240}}\right)^{1/2}} = 0.029 \qquad (2)$$

It is well known that injection at such low Froude numbers is highly unstable. For example, Kuhlman and Prahl[1] found that for $Fr_0 < 0.5$ horizontal injection became unstable and a wedge of ambient fluid entered the injection line (i.e., stratification). We have also observed such counter-current flow phenomena with vertical, upward, injections at $Fr_0 < 0.7$ (see Section 4). Such instabilities in fact may be the reason that data for $Fr_0 < 1$ are essentially non-existent.

This type of instability phenomenon may be viewed as an example of the "lock exchange" problem. Consider, for example, two initially stagnant fluids, side-by-side following the withdrawal of the vertical separating wall. The heavier fluid will form a "nose" which will intrude beneath the lighter fluid sliding along the channel floor. In response

the lighter fluid slides over the "nose" into the space previously occupied by the heavier one. This intrusion velocity, U, seems to be defined by a characteristic value of the Froude number. Inviscid theory yields [2]

$$Fr_c = \frac{U}{(Dg\frac{\Delta\rho}{\rho})^{1/2}} = 0.5 \qquad (3)$$

while the measurements of Barr [3] in completely enclosed wide conduits yielded $Fr_C \sim 0.44$. Clearly the velocity U thus calculated greatly exceeds U_{CL} of Equation (2) hence a nose of ambient downcomer fluid can propagate upstream yielding stratification.

Pertinent in this regard are also the experiments of Keulegan [4]. He observed the shapes of arrested saline wedges having intruded against a fresh water flow in a pipe. At the channel exit the wedge occupied roughly one-half of the channel cross section and gradually reduced in depth with distance from the exit. The total penetration length increased as the initial (fresh water) Froude number decreased being already ~ 40 diameters long at $Fr_0 \sim 0.40$. The shapes and penetration were well predicted by Harleman [5]. For a given initial Froude number, Fr_0, the penetration length may, thus, be estimated by

$$\frac{L}{d} = \frac{1}{4C_o}\left[\frac{1}{5}Fr_o^{-2} - 2 + 3Fr_o^{2/3} - \frac{6}{5}Fr_o^{4/3}\right] \qquad (4)$$

Having shown that the well-mixed cold-leg cannot exist we next turn to the examination of the stability of the stratified regime. It is convenient for this purpose to visualize the process through the initial stages of layer formation. The injected HPI travels downwards continually heating up by entraining and mixing with the ambient fluid. Thus MR1 is characterized by the behavior of a highly turbulent axisymmetric buoyant jet. The decay (heatup) of such jets depends on the distance from the entry point (using the injector diameter as a length scale) and the injection Froude number (see Section 3). Let us take the 2" Westinghouse

injector as an example. With HPI flow at 0.5 ft^3/s and 60°F we estimate $Fr_0 \sim 28$. A maximum of ~14 diameters of travel is available before the jet strikes the opposite wall (bottom of cold leg). The jet would arrive to this point with a mixed mean temperature of ~400°F. It is still significantly heavier than the ambient (550°F) and it will stratify out by spreading (the initial penetration taking the form of a "nose" of the type discussed above) along the bottom of the cold leg (in both directions). However the initial motion as produced by the deflection due to wall impact would be supercritical (Fr > 1) and quickly would undergo a hydraulic jump to a much thicker level. This process is qualitatively illustrated in Figure 2, and its details are not important except that the available travel for the axisymmetric jet would eventually be less than 14d prior to being submerged into the cold layer. That is as the cold layer builds up, it is fed by a continuously colder jet until eventually an equilibrium is established such that all the jet flow is accommodated by the flow in the horizontal stratified layer of the cold leg. It is worth pointing out here that if the injector diameter was large such that $Fr_0 < 1$ counter-current flow and significant mixing within the injector line would occur. The build up of the cold layer within the cold leg would be much more quiet now, till an equilibrium height is again achieved. We now need to show that such equilibrium conditions are indeed realistic.

At the exit of the cold-leg the conditions in the cold stream (cs) and counter flowing stream (hs) must satisfy

$$Fr_{cs}^2 + Fr_{hs}^2 = 1 \qquad (5)$$

For any thickness of the cold layer its temperature and flow may be estimated by assuming they equal that of the feeding axisymmetric jet (at the particular elevation) mixed mean temperature and total flow (including the entrainment) respectively. The flow rate in the hot layer is also known and equal to the total jet entrainment. The two stream Froude numbers may next be estimated to test whether Equation (5) is satisfied.

If not, a new value for the thickness is assumed and this process is continued until consistency with Equation (5) is obtained. We note that $Fr_{cs} > Fr_{hs}$ and that as Fr_{cs} decreases the calculated cold layer temperature also decreases, hence we can bound the behavior by assuming that $Fr_{cs} \sim Fr_{hs}$ and from Equation (5) we obtain $Fr_{cs} \sim 0.7$. For a cold-leg running about half-full with the cold stream, as is usually the case, this is equivalent to $Fr_{cl} \sim 0.5$. Since the results are quite insensitive to this parameter the iteration described above may be considerably simplified by simply requiring that $Fr_{cl} \sim 0.5$. This value is also consistent with the "nose" advancing velocities and intrusion shapes and rates as discussed above. With the cold layer Froude number specified a simple iteration may be carried out such that calculated layer thickness and temperature are consistent with the jet decay characteristics. Typically we find a near half-full cold leg with the cold stream and total entrainment rates that are 2-3 times that of the HPI flow rate.

Next we must address the mixing behavior in MR2. This process is characterized by the pipe Richardson number defined by

$$Ri_p = \frac{D g \frac{\Delta \rho}{\rho}}{U^2} \qquad (6)$$

where U is the relative velocity between the streams and $\Delta\rho \sim \rho_d - \rho_a$ with ρ_d being the density of the fully mixed discharge. Minimal entrainment was found experimentally for a horizontal, fully reversed layer, at $Ri_p > 0.0\,1$ [6]. For the reactor case illustrated in Section 5 and at 350 s, for example, we estimate $Ri_p \sim 5.4$, confirming the persistence of stratification during the horizontal travel between the injection point and the downcomer. This behavior is also confirmed by the CREARE run #64 showing significant stratification in the cold leg (see also Section 4.3).

Finally the cold stream exiting the cold leg will spill over into the downcomer (MR3) to form an essentially planar buoyant jet (MR4) contained within the downcomer walls. This jet will decay as it descends to the lower plenum entraining and mixing with ambient fluid (i.e., growing in the azimuthal direction). We will ignore the mixing in MR3 and will hence utilize cold-leg exit stream properties to characterize the initial conditions for MR4. The characteristic length is obtained assuming that

all the cold stream is deflected downwards, filling up the whole downcomer width with no loss in velocity. This length, ℓ_c, is typically of the order of the cold-leg diameter such that MR4 extends to roughly $\ell/\ell_c \sim 10$. At this length the jet (usually at $Fr_0 \sim 0.6$) would have grown roughly to a lateral dimension of $\sim 2.4\ \ell_c$ (see Section 3) thus occupying only about 40% of the downcomer circumference corresponding to one loop. Ample space is, therefore, available for the flow of the rising plenum fluid making up the quantity of downward flowing entrained quantities.

2.3 Response of the Ambient

The problem of the ambient response due to the injection of a buoyant jet in a confined region has been dealt with by Baines and Turner [7]. They treated explicitly a cylindrical region and found that an equilibrium distribution would soon be established such that the density of the ambient changes in such a fashion that its spatial distribution remains constant. This distribution, quantitatively shown in Figure 3, indicates that to a good approximation the major portion of the density variation is confined within the lower 10%-20% of the container. That is, the ambient behaves as well mixed. Although the geometry in our case is more complicated we expect a behavior essentially similar, while neglecting any ambient stratification is conservative.

We may arrive to the same conclusion also from another view point. As we will see in the next section, the cold stream entering the lower plenum consists of 1 part HPI to 15 parts entrained ambient fluid. This represents a volumetric flow rate of 8 ft^3/s which would require just under one minute to recirculate the 400 ft^3 of lower plenum volume corresponding to one loop. The time constant for changing the temperature of this large volume is considerably longer; thus a quasi-static behavior in a spatially uniform ambient (slowly cooling down) is evident.

3 THE ANALYTICAL TOOLS

Our procedure requires the prediction of the mixed mean temperatures and total entrainments as functions of ℓ/d for axisymmetric buoyant jets, and of the centerline (minimum) temperatures as a function of ℓ/ℓ_c for planar buoyant jets. The jet model of Chen and Rodi [8], Chen and Chen [9],

and Chen and Nikitopoula [10] was adopted for this purpose. The model utilizes the standard equations for natural convection boundary layer type flows with a vertically oriented buoyancy force and a k-ε-$\overline{T'^2}$ differential turbulence model to evaluate the transport terms in the above equations. With the choice of appropriate scales these equations may be put in dimensionless form such that only one main parameter, the Froude number, appears. A small correction due to variation of the thermal expansion coefficient, β, with temperature, several "constants" of the turbulence model and the initial values of the turbulence quantities k, ε, and $\overline{T'^2}$ also appear. The resulting system of equations is summarized below, where i = 1 for axisymmetric and i = 0 for planar geometry.

$$x^* = \frac{x}{d} \quad (8) \qquad y^* = \frac{y}{d} \quad (9)$$

$$u^* = \frac{u}{u_{of}} \quad (10) \qquad v^* = \frac{v}{u_{of}} \quad (11)$$

$$T^* = \frac{T - T_a}{T_{of} - T_a} \quad (12) \qquad \epsilon^* = \frac{\epsilon}{u_{of}^3/d} \quad (13)$$

$$k^* = \frac{k}{u_{of}^2} \quad (14) \qquad \overline{T'^2}^* = \frac{\overline{T'^2}}{(T_{of} - T_a)^2} \quad (15)$$

$$Fr = \frac{u_{of}}{\sqrt{g\beta d(T_{of} - T_a)}} \quad (16)$$

$$\frac{\partial u^*}{\partial x^*} + \frac{1}{y^{*i}} \frac{\partial}{\partial y^*}(y^{*i} v^*) = 0 \quad (17)$$

$$u^* \frac{\partial u}{\partial x^*} + v^* \frac{\partial u^*}{\partial y^*} = \frac{1}{y^{*i}} \frac{\partial}{\partial y^*}(-y^{*i} \overline{uv}^*) + \frac{T^*}{Fr^2} \frac{\beta(T_{of})}{\beta(T)} \quad (16)$$

$$u^* \frac{\partial T^*}{\partial x^*} + v^* \frac{\partial T^*}{\partial y^*} = \frac{1}{y^{*\alpha}} \frac{\partial}{\partial y^*} \left(-y^{*\alpha} \overline{vT'^*} \right) \tag{19}$$

$$u^* \frac{\partial K^*}{\partial x^*} + v^* \frac{\partial K^*}{\partial y^*} = \frac{1}{y^{*\alpha}} \frac{\partial}{\partial y^*} \left(y^{*\alpha} C_K \frac{K^* \overline{v^2}^*}{\epsilon^*} \frac{\partial K^*}{\partial y^*} \right) - \overline{uv}^* \frac{\partial u^*}{\partial y^*} + \frac{\overline{uT}^*}{F_r^2 \frac{\beta(T_{0\infty})}{\beta(T)}} - \epsilon^* \tag{20}$$

$$u^* \frac{\partial \epsilon^*}{\partial x^*} + v^* \frac{\partial \epsilon^*}{\partial y^*} = \frac{1}{y^{*\alpha}} \frac{\partial}{\partial y^*} \left(y^{*\alpha} C_\epsilon \frac{K^* \overline{v^2}^*}{\epsilon^*} \frac{\partial \epsilon^*}{\partial y^*} \right) + C_{\epsilon 1} \frac{\epsilon^*}{K^*} \left(-\overline{uv}^* \frac{\partial u^*}{\partial y^*} + \frac{\overline{uT}^*}{F_r^2 \frac{\beta(T_{0\infty})}{\beta(T)}} \right) - C_{\epsilon 2} (1 - 0.035G) \frac{\epsilon^{*2}}{K^*} \tag{21}$$

$$u^* \frac{\partial \overline{T'^2}^*}{\partial x^*} + v^* \frac{\partial \overline{T'^2}^*}{\partial y^*} = \frac{1}{y^{*\alpha}} \frac{\partial}{\partial y^*} \left(y^{*\alpha} C_T \frac{K^*}{\epsilon^*} \frac{\partial \overline{T'^2}^*}{\partial y^*} \right) - 2 \overline{vT}^* \frac{\partial T^*}{\partial y^*} - C_T \epsilon^* \frac{\overline{T'^2}^*}{K^*} \tag{22}$$

$$-\overline{uv}^* = \frac{1 - C_0}{C_1} \frac{\overline{v^2}^*}{K^*} \left[1 + \frac{K^* \frac{\partial T^*}{\partial y^*}}{F_r^2 \frac{\beta(T_{0\infty})}{\beta(T)} C_h \epsilon^* \frac{\partial u^*}{\partial y^*}} \right] \frac{K^{*2}}{\epsilon^*} \frac{\partial u^*}{\partial y^*} (1 - 0.465G) \tag{23}$$

$$\overline{v^2}^* = C_2 K^* \tag{24}$$

$$-\overline{vT'}^{*} = \frac{1}{C_h}\frac{\overline{v^2}^{*}}{\kappa^{*}}\frac{\kappa^{*2}}{\epsilon^{*}}\frac{\partial T^{*}}{\partial y^{*}} \tag{25}$$

$$\overline{uT'}^{*} = \frac{\kappa^{*}}{C_h\epsilon^{*}}\left[-\overline{uv}^{*}\frac{\partial T^{*}}{\partial y^{*}} - \overline{vT'}^{*}(1-C_{h_1})\frac{\partial u^{*}}{\partial y^{*}} + \frac{(1-C_{h_1})}{F_r^{2}}\frac{\beta(T_a)}{\beta(T)}\overline{T'^{2}}^{*}\right] \tag{26}$$

$$G = \left|\frac{y^{*}_{0.5u^{*}}}{2U_f^{*}}\left(\frac{dU_f^{*}}{dx^{*}} - \left|\frac{du_f^{*}}{dx^{*}}\right|\right)\right|^{0.2} \tag{27}$$

where:

$$C_0 = 0.55 \quad C_1 = 2.2 \quad C_2 = 0.53 \quad C_\epsilon = 0.15$$

$$C_{\epsilon 1} = 1.43 \quad C_{\epsilon 2} = 1.92 \quad C_\kappa = 0.115 \quad C_T = 0.13$$

$$C_{T1} = 1.25 \quad C_h = 3.2 \quad C_{h_1} = 0.5 \tag{28}$$

and:

$$x^{*} > 0 \qquad y^{*} \longrightarrow \infty \qquad T^{*} = u^{*} = \kappa^{*} = \epsilon^{*} = \overline{T'^{2}}^{*} = 0$$

$$x^{*} > 0 \qquad y^{*} = 0 \qquad \frac{\partial}{\partial y^{*}}\left[T^{*}, u^{*}, \kappa^{*}, \epsilon^{*}, \overline{T'^{2}}^{*}\right] = 0$$

$$\text{at } x = 0 \qquad T^{*} = 1 \quad u^{*} = 1 \quad \kappa^{*} = \kappa_0^{*}, \ \epsilon^{*} = \epsilon_0^{*}, \ \overline{T'^{2}}^{*} = \overline{T_0'^{2}}^{*} \tag{29}$$

This system of equations does not describe the impact phenomena (and expected roll-over due to the cold leg curvature) at the cold leg wall opposite to the injection point. Careful investigation of such possible momentum flux effects would be required as a complement of the approach developed here.

The integrations were carried out using the Patankar-Spalding method with 35 radial nodes for the half-jet. Initial values for the dimensionless turbulence properties were set at 0.0125 following the suggestion of Chen and Nikitopoulos [10].

Results for the range of Froude numbers of interest here are presented in Figures 4, 5 and 6. From Figures 4 and 5 we can see the dramatic increase in entrainment and associated jet decay as the Froude number decreases. Figure 6 illustrates the rapid decay of the planar, downcomer jet, yielding a rapid heatup of its centerline temperatures especially in the region $\ell/\ell_c > 2$.

4 THE EXPERIMENTAL BASIS

The general adequacy of the jet model utilized here has been documented by Chen, Rodi, and co-workers [8,9,10] against available experimental data. The nature of the agreement obtained for axisymmetric jets is illustrated in Figure 7. For planar jets the data are scarce especially at the lower range of Froude numbers. In Figure 8 predictions are compared to experimental data as surmised by the correlating scheme of Chen and Rodi [8]. The actual data upon which this correlating line was obtained to not extend below Fr $\sim$1.5. Also for axisymmetric jet no data for Fr < 1 have been published. We have recently obtained some data at Fr = 0.35 and 0.7 in the experimental facility described in [11] and [12]. A honeycomb injector to produce local (within each pore) $Fr_0 > 1$ and hence stabilize the injection was utilized. The quality of the predictions, against these data is illustrated in Figure 9. It should be mentioned that these comparisons are preliminary and in any case that the predictions are conservative (giving slower decay, i.e., lower temperatures) with respect to these data.

The integral aspects of our approach were tested against Run #64 of the CREARE test program [13]. This was the only run with a prototypical density ratio (achieved by injecting a saline solution) and close simulation of the cold-leg Froude number. The geometry of these tests was somewhat ambiguous regarding the ambient response. An unquantified saline solution flowed back past the perforated plate (pump simulator) while in the absence of a lower plenum the degree of recirculation "around" the "hoses" connecting the bottom of the downcomer with the overflow tank remains unclear.

The equivalent of these effects is that one-half of the HPI flow mixes with the cold-leg and downcomer volume to produce an ambient cooldown in close agreement to that measured. Based on this ambient an adequate prediction of cold-leg and downcomer temperature transients is obtained as shown in Figure 10.

5 REACTOR PREDICTIONS

Finally, the approach was applied to a 3-loop Westinghouse PWR plant. A volume (cold-leg, downcomer, and low plenum) of $V_a \sim 760$ ft^3, and all the HPI flow (0.5 ft^3/s), was utilized as the basis of the ambient transient, T_a

$$\frac{T_a - T_{HPI}}{T_{a,0} - T_{HPI}} = e^{-\frac{Q_{HPI}}{V_a} t} \qquad (30)$$

No metal heat was taken into account (a correction easily to be made at a later time). The variation of the control volume mass due to density variation was not taken into account. This at most is a 20% effect and is is believed to just about cancel a similar, at most, ~20% effect due bo backflow of HPI into the loop seal. The calculation was carried out with the help of Figures 4, 5, 6, and hand calculations; i.e., for snapshot in time the particular ambient temperature was used to assemble the regional mixing model by the jet decay curves and the Froude number criteria of Section 2.2 (see Appendix for an example). A sufficient number of such snapshots produce the complete temperature transients as shown in Figure 11. It should be noted that here for similicity the variation of injection Froude number due to ambient temperature variation was not taken into account and the injection Froude number 28 (i.e., roughly in the mid of the actual range of Fr ~17 to 70) corresponding to T_a = 360°F was used for the whole transient. A rather slow cooldown but with significant stratification are predicted. The cooldown observed in the cold leg during the first few minutes is a consequence of such stratification phenomena. Due to the rapid character of this cooldown (controlled by advancing "nose" phenomena discussed earlier) compared to the rest of the transient it did not appear worthwhile to resolve it in any great detail.

6 CONCLUSIONS

The important point made is that stratification rather than perfect mixing controls the response. However, as a consequence of stratification large scale circulations are set up that cause the participation of the HPI fluid with all the primary fluid between the pumps and the core inlet, i.e., a large thermal inertia controls the ambient temperature response. Due to geometry and conditions on the other hand the stratified layers do not represent precipitateously colder regions, i.e., they follow within 50%-100°F the ambient temperature.

Based on these concepts an analytical procedure has been devised which with the help of jet decay curves of the type supplied here reduce the whole prediction to a simple exercise in hand calculations. Additional experimental data on jet decay at low Froude numbers ($Fr_0 < 1$) and exploration of momentum flux effects would be required to put the proposed approach on a firmer basis.

ACKNOWLEDGEMENTS

Financial support for the computer work was donated by Purdue University. We are grateful to Mrs. W. Bauman for making the timely preparation of this manuscript possible.

NOMENCLATURE

C_D = drag coefficient

D_{cl} = cold leg diameter

d = HPI jet diameter

e = basis of the natural logarithm

F_r = Froude number = $u/(gd\frac{\Delta\rho}{\rho})^{1/2}$ or $\frac{u}{\sqrt{g\beta d(T_d - T_a)}}$

$F_{r_{cl}}$ = cold leg Froude number based on velocity of cold stream and cold leg diameter

$F_{r_{cs}}$ = cold stream Froude number based on height and velocity of the cold stream

$F_{r_{hs}}$ = hot stream Froude number based on height and velocity of the hot stream

g = acceleration of gravity

K = turbulent kinetic energy = $\overline{u_i u_i}/2$

K^* = $K/u_{0_d}^2$

ℓ_c = width of planar buoyant jet at the cold leg/downcomer junction

Q = flow rate

R_{i_p} = pipe Richardson number = $\frac{Dg\frac{\Delta\rho}{\rho}}{u^2}$

T = mean jet temperature

T^* = $\frac{T - T_a}{T_{0_d} - T_a}$

T' = fluctuating jet temperature

T_a = ambient temperature

T_{cl} = mean cold leg temperature

T_{cl_0} = initial mean cold leg temperature

T_{HPI} = HPI temperature

T^*_{mean} = mixed mean axisymmetric jet temperature

t = time

u = jet mean velocity component in the axial direction

u^* = u/u_{0_d}

U_{cl} = superficial velocity in cold leg

V_{cl} = cold leg volume

v = mean velocity component in the normal direction

$\nu^* = \frac{\nu}{u_{oj}}$

x = axial direction of the buoyant jet

x^* = x/d

y = normal direction of the jet from symmetric axis

y^* = y/d

$y_{.5u}$ = distance from the centerline to the point where the velocity is half of the centerline velocity

Greek Symbols

β = thermal coefficient of volumetric expansion

$\Delta\rho = \rho - \rho_a$

ϵ = dissipation rate of the turbulent kinetic energy

$\epsilon^* = \epsilon/(u_{oj}^3/d)$

ρ = density

ρ_a = local ambient density

$\rho^* = \frac{\rho - \rho_a}{\rho_o - \rho_a}$

Subscripts

a = ambient condition

CL = cold leg

CS = cold stream

HS = hot stream

HPI = high pressure injection condition

ℓ = centerline value

o = initial value

REFERENCES

1. Kuhlman, J. K. and J. M. Prahl, J. Great Lakes, Res., 1, 1, 101 (1975).

2. Turner, J. S., Buoyancy Effects in Fluids, Cambridge Univ. Press (1973).

3. Barr, D. I. H., La Houille Blanche, 6101 (1967).

4. Keulegan, G. H., Nat. Bur. Stand., Report 5482 (1957).

5. Harleman, Stratified Flow in Handbook of Fluid Mechanics (ed. V. L. Streeter) Ch. 26, McGraw Hill (1961).

6. Ellison, T. H. and J. S. Turner, J. Fluid Mechanics 8, 514 (1960).

7. Baines, W. D. and J. S. Turner, J. Fluid Mechanics 37, Part I, 51 (1969).

8. Chen, C. J. and W. Rodi, Vertical Turbulent Buoyant Jets, Pergamon Press (1979).

9. Chen, C. J. and C. H. Chen, J. Heat Transfer 101, 532 (1979).

10. Chen, C. J. and C. P. Nikitopoula, Int. J. Heat Mass Transfer 22, 245 (1979).

11. Theofanous, T.G., PNE-80-147, Purdue University (1980).

12. Theofanous, T.G., NUREG/CR-2318 (1981).

13. Rothe, P. H. and M. F. Ackerson, EPRI NP-2312 (1982).

APPENDIX: Sample Calculation for Reactor Predictions

Here a sample calculation of regional mixing model applied to a 3-loop Westinghouse PWR plant is presented. Taking 750 seconds following HPI actuation the ambient temperature, T_a = 359°F, is obtained from equation (20). By iteration a height ∿0.83 ft for cold stream is found to meet the Froude number criterion discussed in Section 2.2, i.e. Fr_{CL} = 0.5. This is done as follows: A height of 0.83 ft for the cold stream corresponds to $\ell/d \sim 9$ ($\ell/d = (2.33 - .83)/(2/12) \sim 9$) and referring to Figure 4 ($Fr = U_{HPI}/\sqrt{gd\frac{\Delta\rho}{\rho}} \sim 28$)

$$T^{*}_{MIX} = \frac{T_{CS} - T_a}{T_{HPI} - T_a} = 0.35$$

or $T_{CS} = 0.35\ (60 - 359) + 359 \sim 254°F$

Now we use Figure 5 to obtain

$$\frac{Q}{Q_{HPI}} = 2.85$$

or $Q = 2.85 \times 0.5 = 1.425\ ft^3/s$

The cross sectional area of cold stream A_{cs} corresponding to a cold stream height h ∿83ft is 1.33 ft^2, $\left(A_{cs} = \alpha D^2/4 - (D/2 - h)\sqrt{h(D-h)}\right.$ where $\left.\alpha = \arctan\left(\frac{\sqrt{h(D-h)}}{D/2 - h}\right) \text{ in radians}\right)$

The velocity and Froude number of cold stream are obtained as

$$u_{cs} = \frac{Q}{A_{cs}} = \frac{1.425}{1.33} \approx 1.07\ ft/sec$$

$$Fr_{CL} = \frac{u_{cs}}{\sqrt{gD\frac{\Delta\rho}{\rho}}} = \frac{1.07}{\sqrt{32.2 \times 2.33 \times 0.059}} \approx 0.5$$

Assuming that all the cold stream is deflected downwards, filling up the whole downcomer width, W_d, with no loss in velocity, U_{CS}, then the width of planar jet ℓ_c at the cold leg/downcomer junction is obtained as

$$\ell_c = \frac{Q}{W_d u_{cs}} = \frac{1.425}{0.792 \times 1.07} \approx 1.68\ ft$$

Referring to Figure 6 the downcomer temperature along the jet axis (coldest locations) at positions 1.2 and 3 is obtained from the dimensionless centerline temperatures $\left(T^{\circ}_{\ell} = \frac{T_{\ell} - T_a}{T_{cs} - T_a}\right)$ Corresponding to their ℓ/ℓ_c values

Location 1	$\ell/\ell_c = 1.66$	$T_{c1} = 257°F$
2	$\ell/\ell_c = 6.2$	$T_{c2} = 322°F$
3	$\ell/\ell_c = 10.6$	$T_{c3} = 341°F$

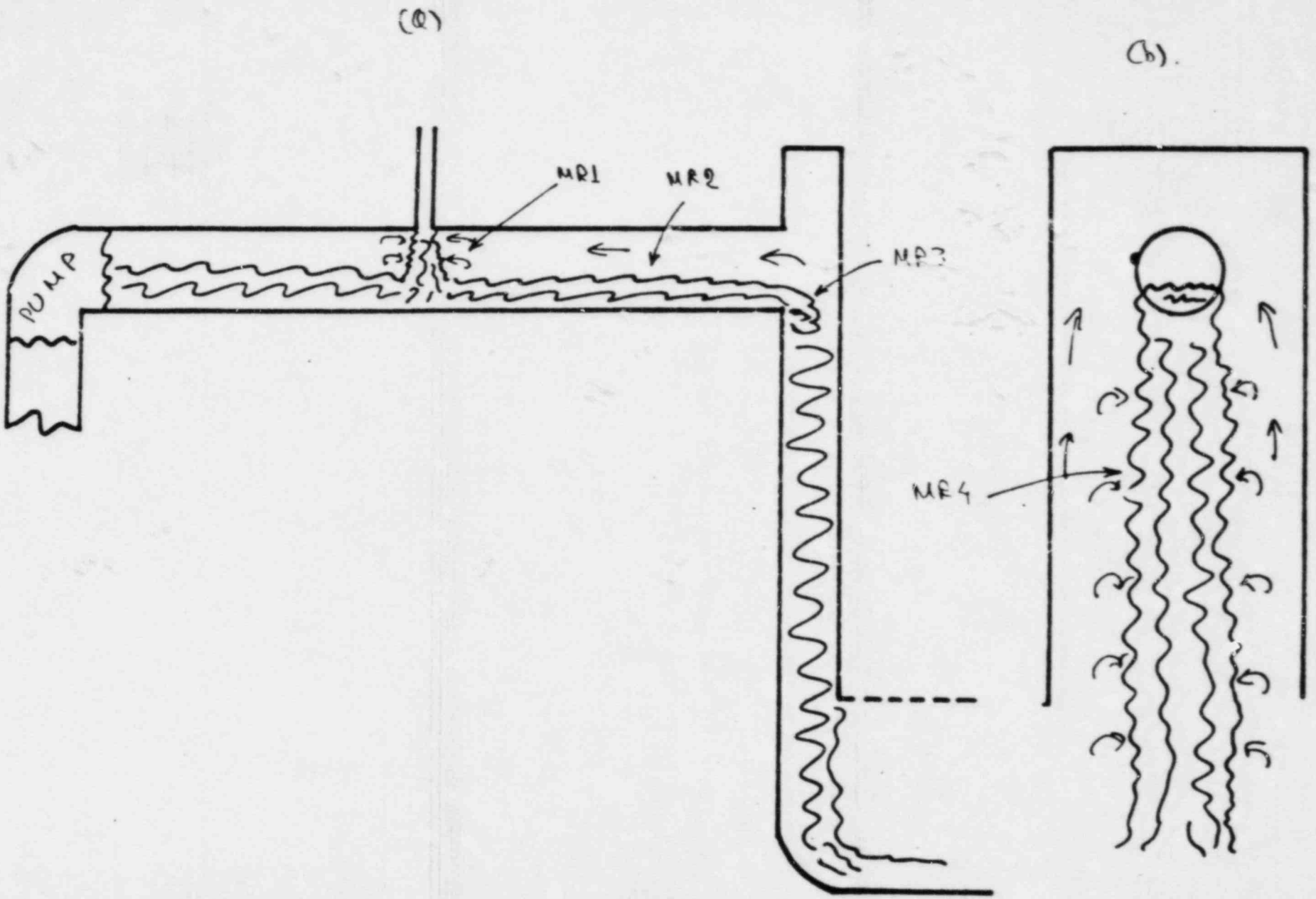

Fig. 1. The geometry of mixing regions (MRs).

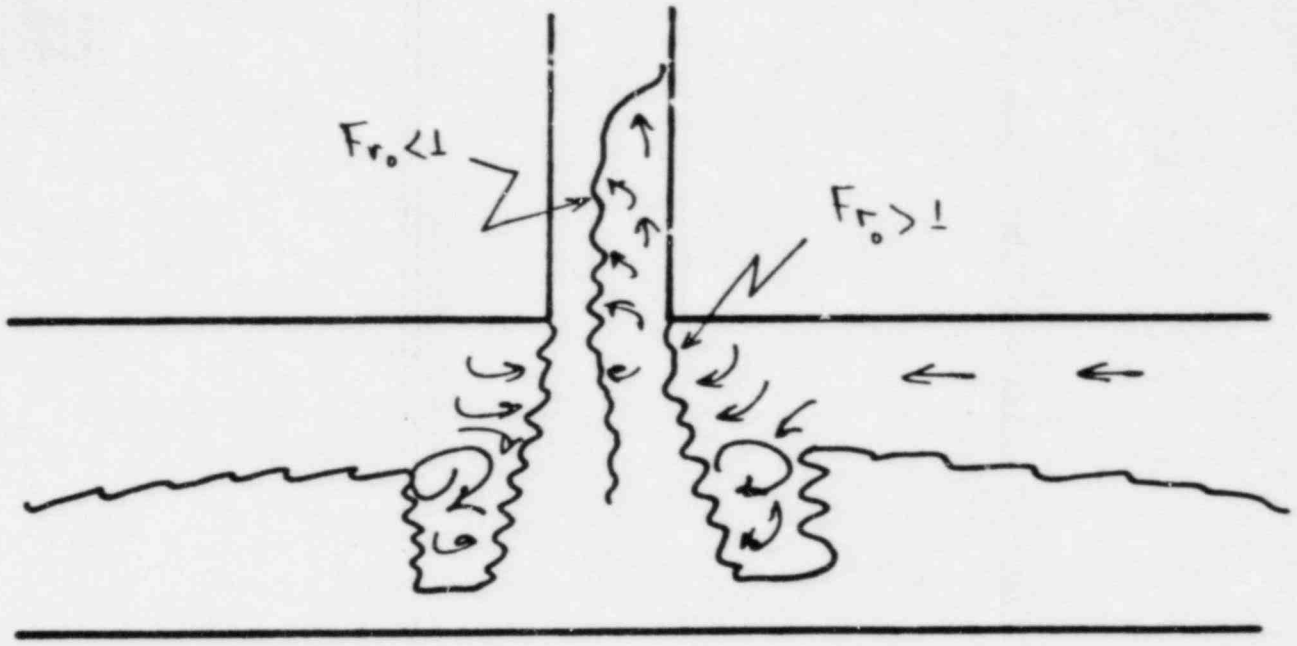

Fig. 2 **Flow regimes at Mr1.**

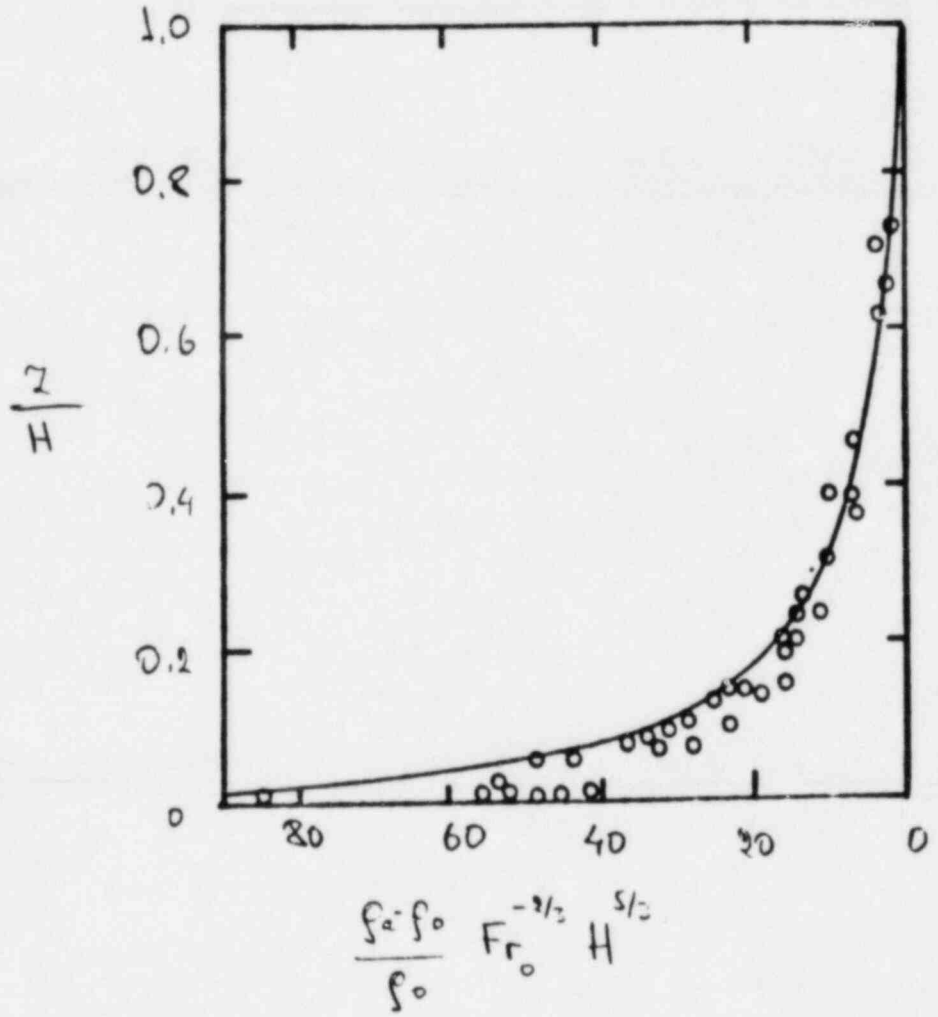

Fig 3 Distribution of density at "equilibrium conditions.

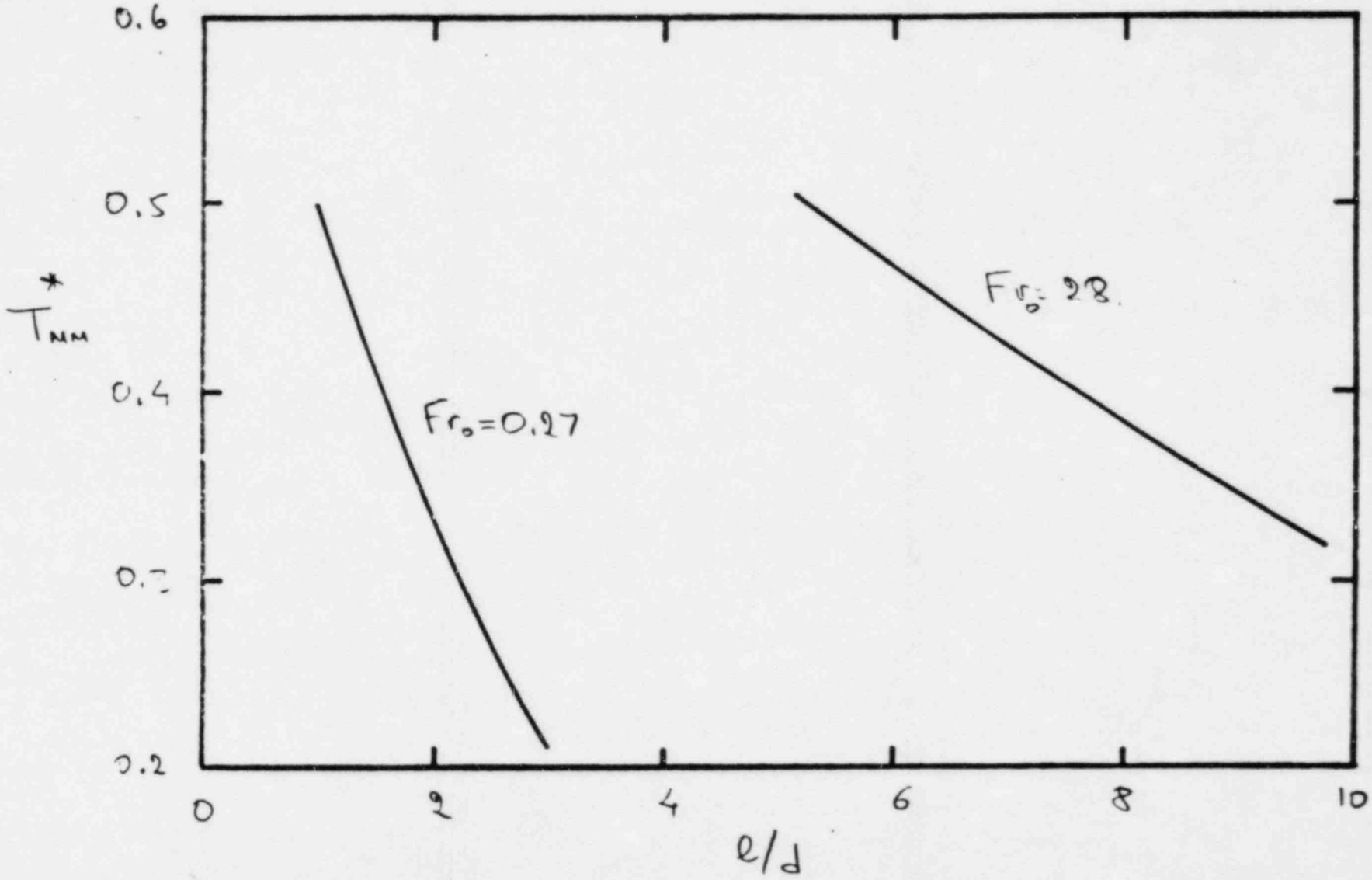

Fig. 4 **Prediction of mixed mean axisymmetric jet temperature as a function of ℓ/d and Fr_o.**

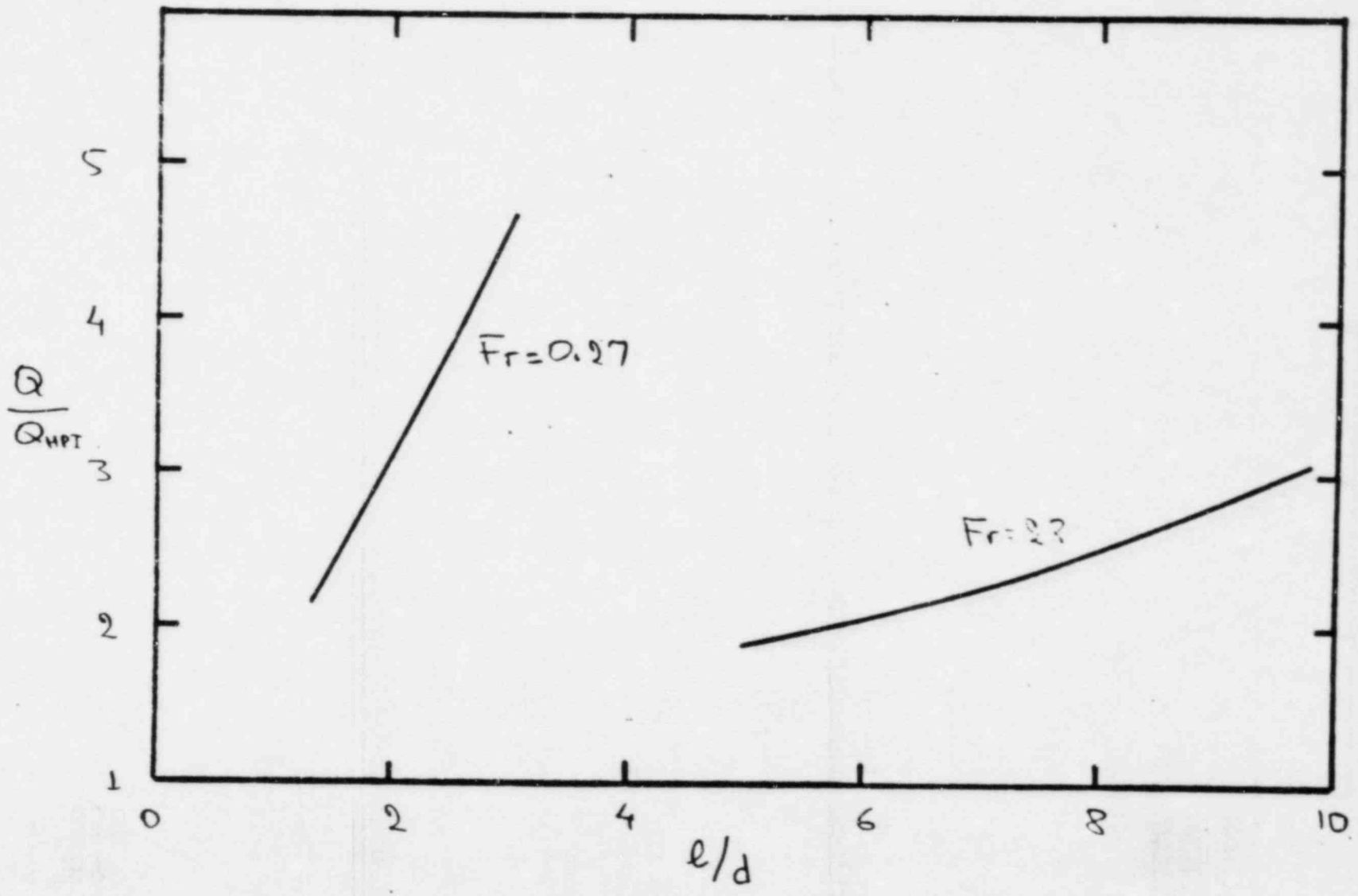

Fig. 5 Prediction of total flow for axisymmetric jets as a function of ℓ/d and Fr_0.

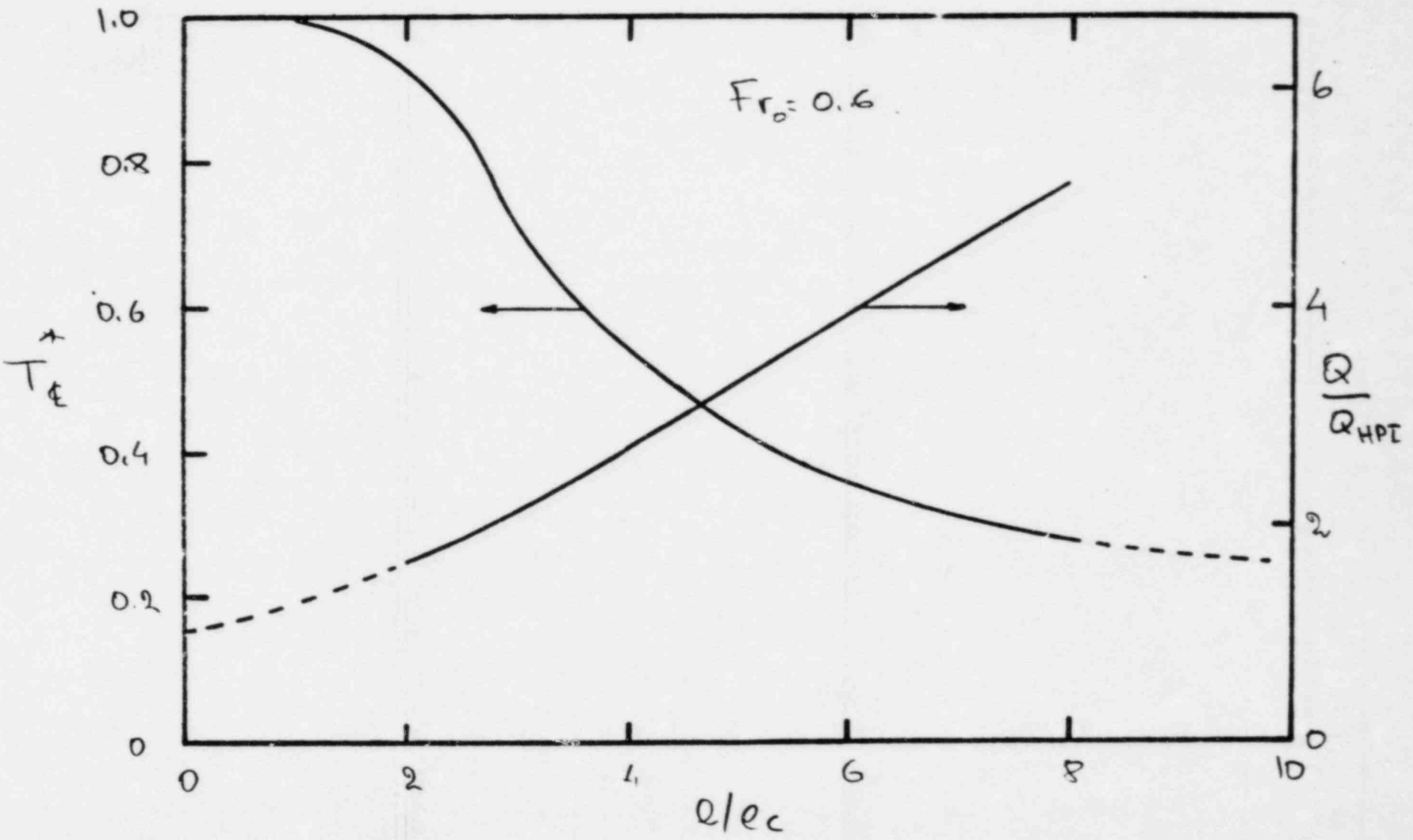

Fig. 6 Predictions of centerline temperature and for planar jets as function of ℓ/d_c total flow.

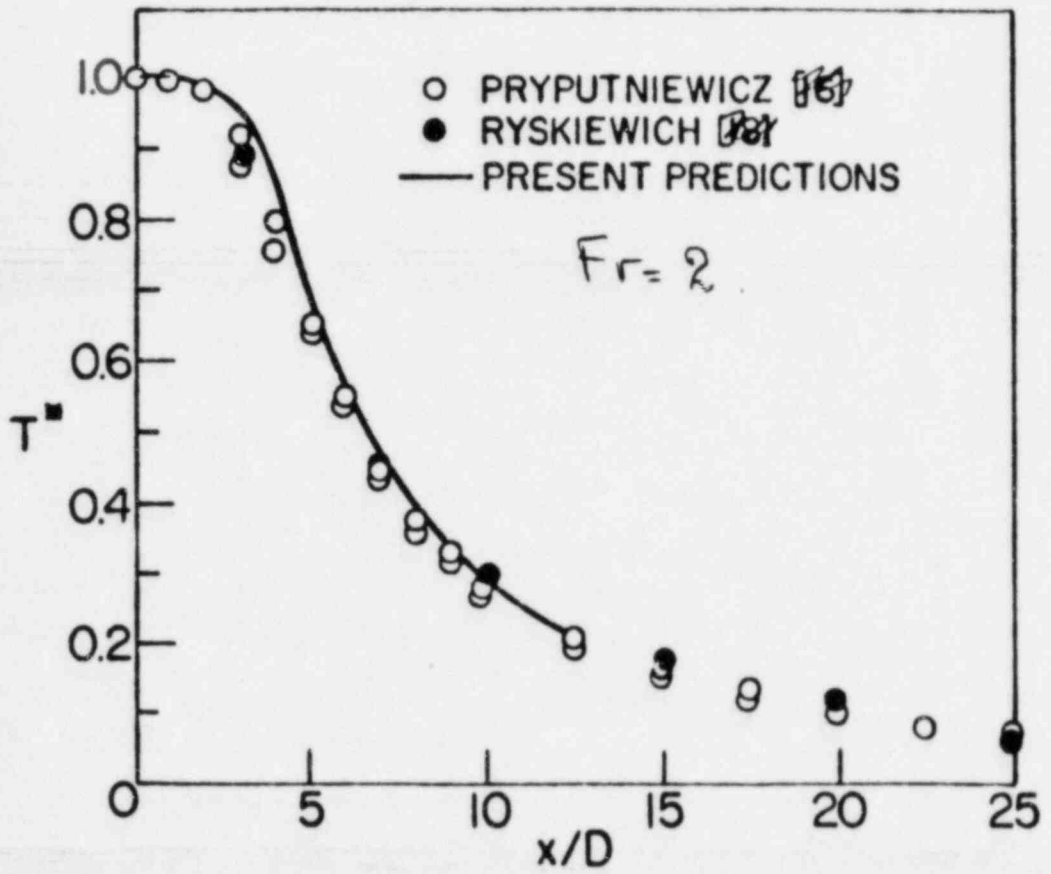

Fig. 7 Comparisons of prediction with the data for axisymmetric jet.

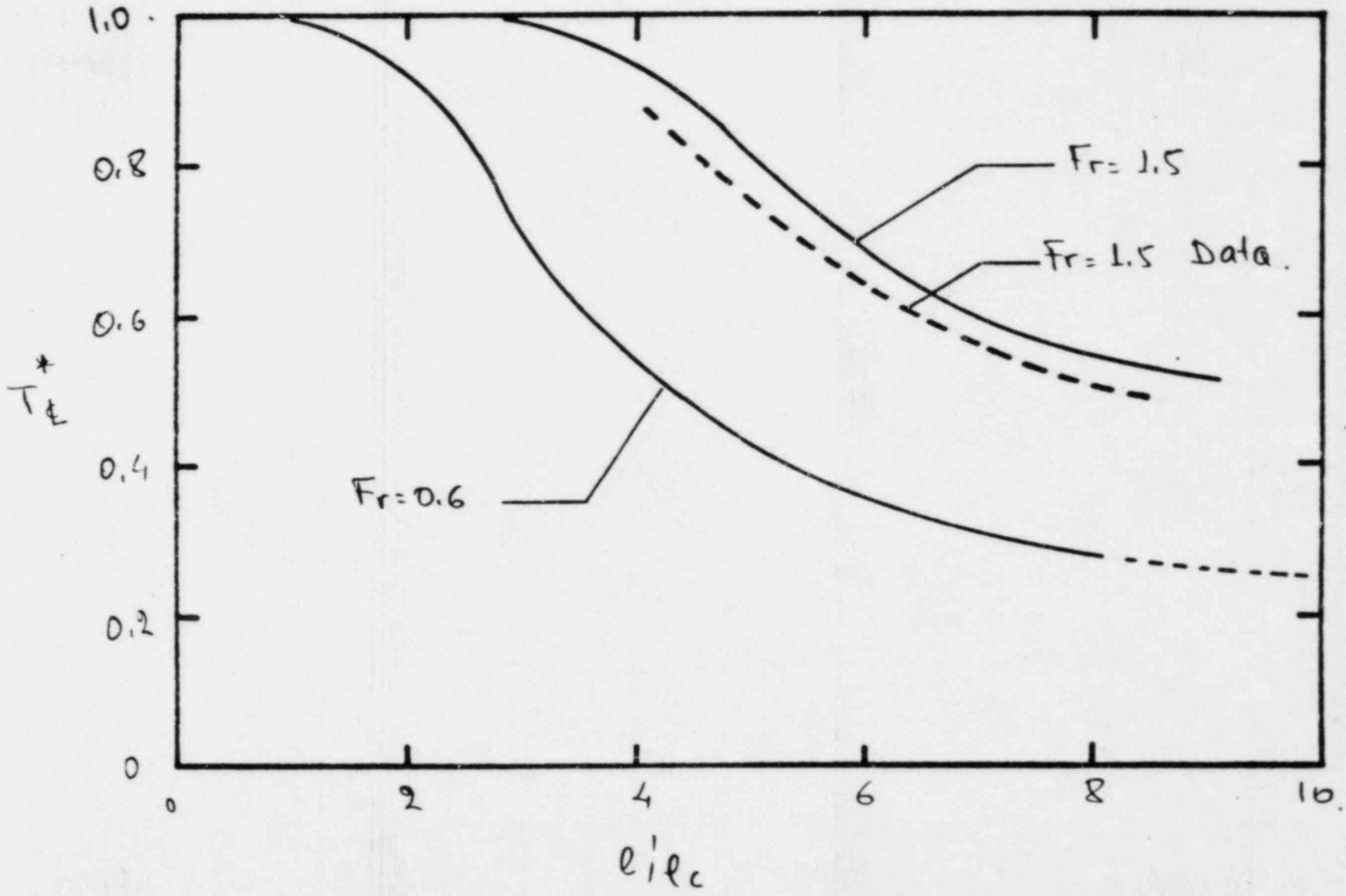

Fig. 8 Comparisons of predicted (——) planar jet decay with available data as represented by the Chen & Rodi correlation. Prediction for $Fr_0 = 0.6$ for which no data are available is also shown for comparison.

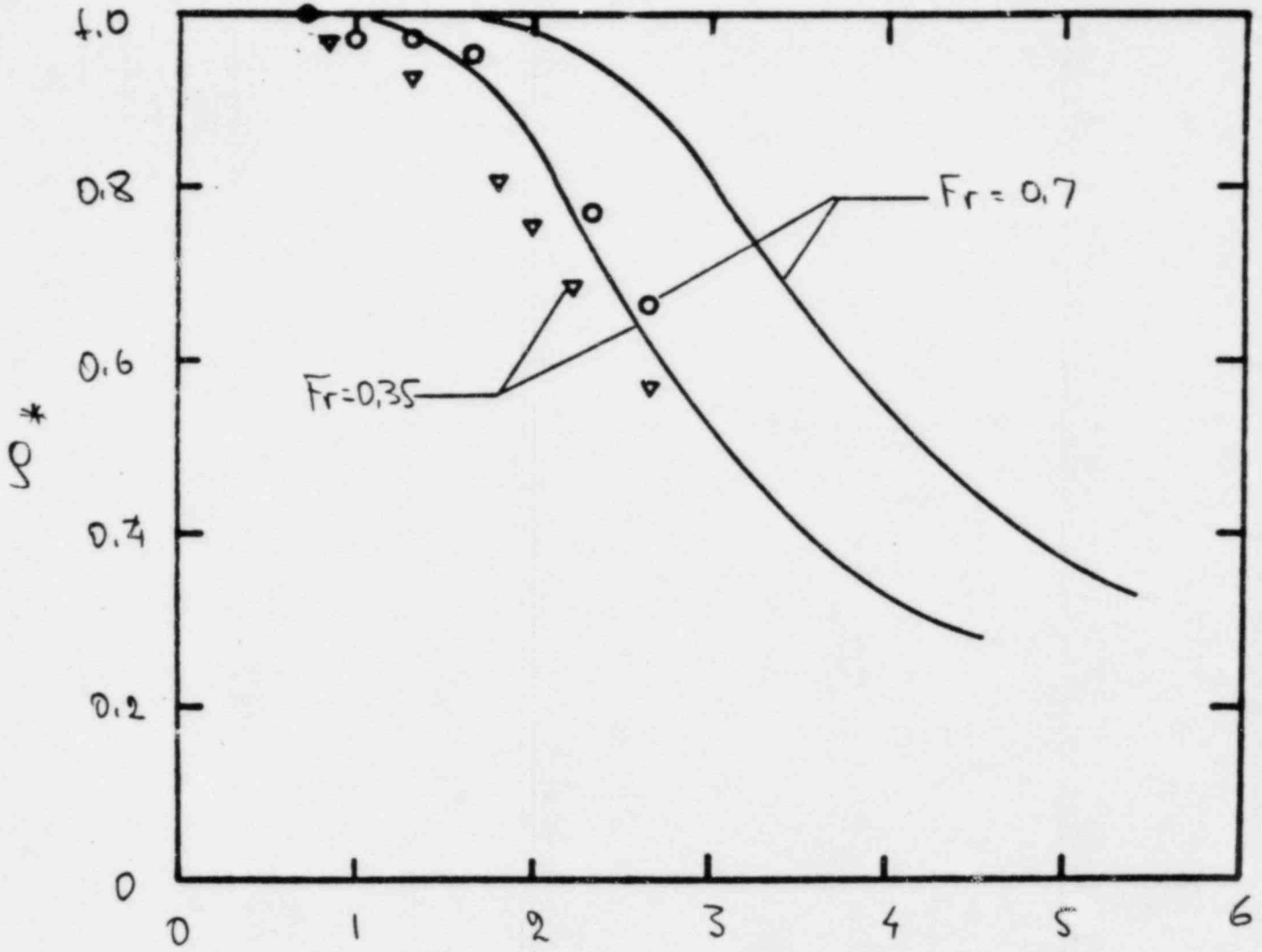

Fig. 9 Comparison of predicted axisymmetric jet decay against our currently obtained experimental data.

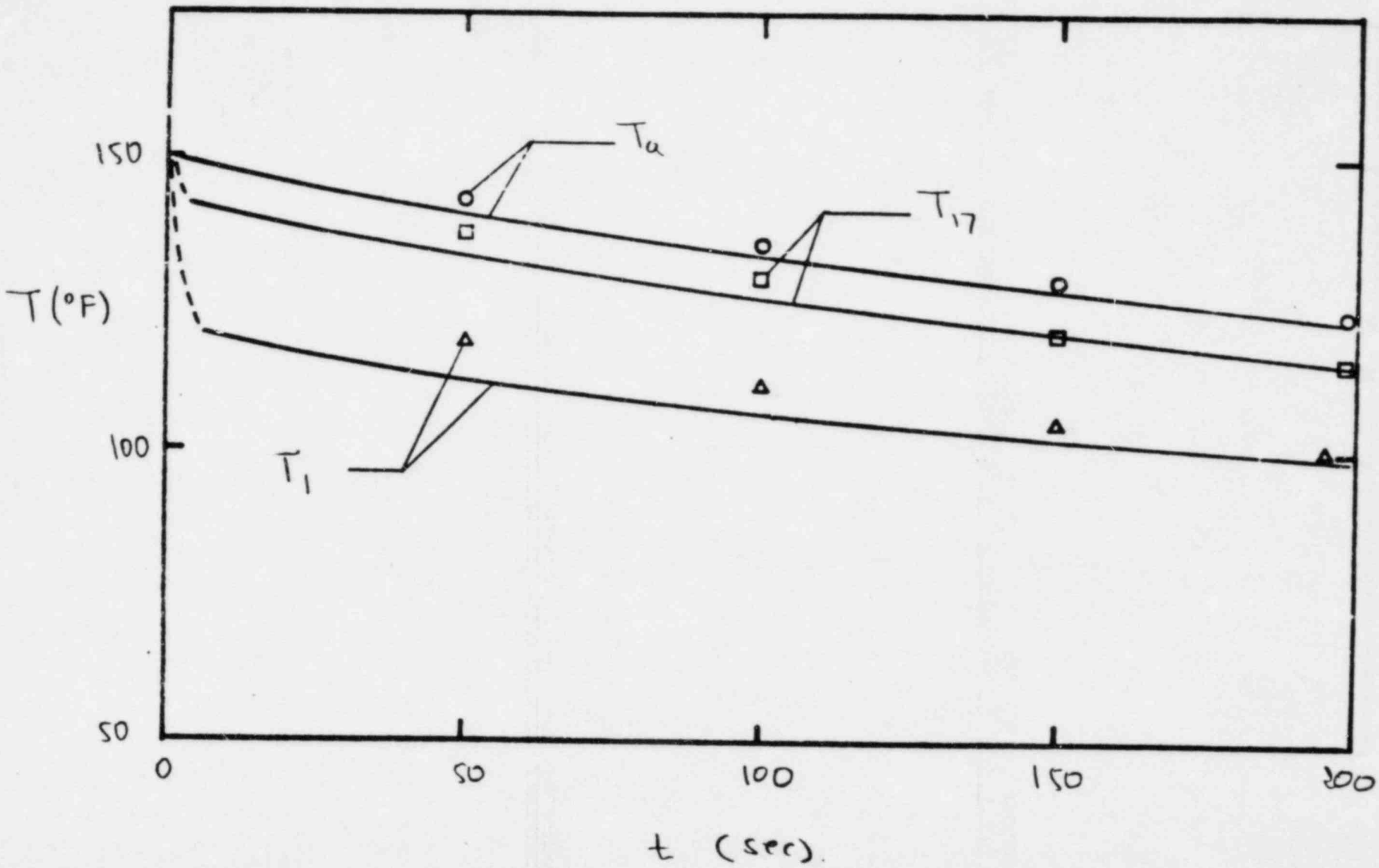

Fig. 10 Predictions (——) of CREARE test #64 temperature transients against the data.

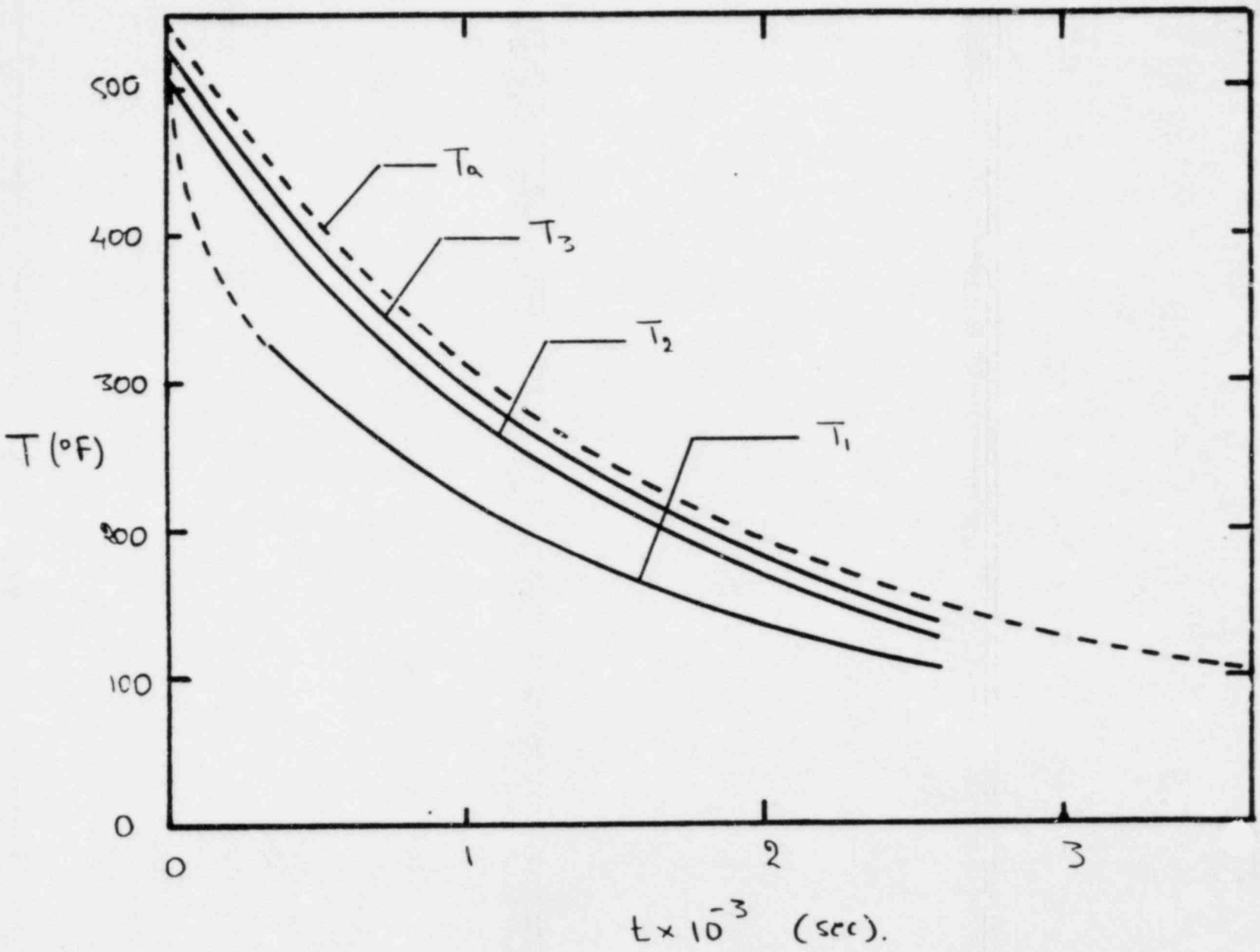

Fig. 11 **Prediction of temperature transients in a 3-Loop Westinghouse PWR Plant. T_1, T_2, T_3 temperatures at top, middle, and bottom of core elevation.**